Journal of Alloys and Compounds 585 (2014) 393–397

Contents lists available at ScienceDirect

Journal of Alloys and Compounds

journal homepage: www.elsevier.com/locate/jalcom

Role of Au nanoparticle aggregation in laser induced anisotropy of ITO transparent substrates

I.V. Kityk [a,*], J. Ebothe [b], N-B. Bercu [b], Md. Abdul Aziz [c], Munetaka Oyama [d]

[a] Electrical Engineering Department, Czetochowa University Technology, Armii Krajowej 17, Czestochowa, Poland
[b] Laboratoire de Recherche en Nanosciences, E.A. 4682, Université de Reims, 21 rue Clément Ader, 51685 Reims cedex 02, France
[c] Center of Research Excellence in Nanotechnology, King Fahd University of Petroleum and Minerals, Dhahran 31261, Saudi Arabia
[d] Department of Material Chemistry, Graduate School of Engineering, Kyoto University, Nishikyo-ku, Kyoto 615-8520, Japan

ARTICLE INFO

Article history:
Received 10 September 2013
Received in revised form 20 September 2013
Accepted 20 September 2013
Available online 30 September 2013

Keywords:
Silver nanoparticle morphology
Photoinduced treatment of the nanocomposite surfaces

ABSTRACT

A principal possibility to achieve the photoinduced anisotropy in the Au NP deposited onto the ITO substrate is experimentally shown. The sizes of the Au NP forming the corresponding nanocomposites were 20 nm, 30 nm and 40 nm. As a photoinducing light source we have used two coherent beam originating from the Er:glass laser generating at 1540 nm with frequency repetition 15 Hz as well as its second harmonic doubled frequency signal at 770 nm. The effect is sensitive to the angle between the two laser beams as well as to the Au NP sizes, inter-particle distances and topology connected with their aggregation. The effect shows slow relaxation to the initial state. The optimal conditions are achieved for nanocomposites formed by 30 nm despite the expected 20 nm. This one may be caused by crucial role of the partial aggregation which even changes the effective grain sizes. The contribution of the dipole–dipole as well as quadrupole–dipole interactions to the changes of the anisotropy is discussed. The excitation is far from the resonance which allow to predict that effective role play overlap with nanotrapping levels. So principal role may belongs to surface topology and which is studied using the birefringence directly connected with the anisotropy.

1. Introduction

Recently in the photonics there occurred several works devoted to decrease of parasitic reflectance of materials during its interaction with the visible light [1–4]. There are two principal kind of the light scattering: the forward and backward ones which depend not only on the inter-particle distance however additional role play here the aggregation and effective contact surfaces between the nanoparticles (NP) and the substrates. Generally the forward component is enhanced with the decreasing the contact area between the NP and the dielectric substrate. Also the contact area with the substrate (particle size and shape). It was established that that metal hemispheres show significant backscattering and reduced back scattering. Additionally one can expect some anisotropy between the forward and the backscattering components. Most of the works in this direction were performed for the studies of the reflectance decrease [5,6].

However, in this case we deal mainly with the particular photo generated media. However the role of the electrodes like transparent ITO usually is neglected. At the same time in the Ref. [7]. It was shown that applying a special seed-mediated technique one can achieve some phase modulation related to birefringence (additionally to reflection/absorption). The later in turn will be very promising for the operation of the losses like in the thin film phase plate films.

As a consequence in the present work we will perform the study of possibility to vary the refractive indices for the Au NP trough measurements of the optical birefringence in the visible spectral range applying the external laser light. In the Ref. [8] it was shown that such possibility is more effective during the use of the bicolor coherent beams, like the fundamental and its doubled frequency. As a source of the fundamental beam we have chosen the Nd:YAG nanosecond laser and its second harmonic generation as well as Er:glass laser together with its doubled frequency beam.

We have used gold NP of different sizes deposited on the ITO electrode substrate using the technique described in the Ref. [9]. However, contrary to previous works we will explore the changes of the light phase through measurements of refractive indices changes. The exceptional features of plasmonic noble metals to gather light due to overlap of surface plasmon resonance (SPR) excitations and of the effective nanotrapping levels on the substrates. Plasmonic low-dimensional features of gold NP together with semiconductors like ITO with energy gap above 3.2 eV should allow substantially decrease the light losses and concentrate the more part of the light within the photovoltaic solar cell device

* Corresponding author. Tel.: +48 343221841.
E-mail addresses: iwank74@gmail.com, ikityk@el.pcz.czest.pl (I.V. Kityk).

0925-8388/$ - see front matter © 2013 Elsevier B.V. All rights reserved.
http://dx.doi.org/10.1016/j.jallcom.2013.09.143

may be a principal strategy for the further development f the solar cell devices. So the main task is to find the maximal overlap between the SPR and the incident photons. However, this task will be achieved by additional laser treatment of the such kind of nanocomposites.

Following the general theory of interaction of the light and the metallic nanostructures with semiconductors [1,10–12] one can expect that there are many factors like average sizes, inter-particle distances, however for the photoinduced case the additional important factor will be topology and their effective polarizability. As a consequence in the present work we will explore in details the topology of the Au NP and we will try to perform the illumination by the two laser sources (1064 nm and 1540 nm) to show how spectrally sensitive will be the changes.

From another side contrary to silicon derivatives the ITO films are in principle dielectric with effective energy gap up to 3.2 eV. So they are transparent for the larger amount of the light. Taking into account that recently it was developed effective seed—mediated technology of covering these films by the Ag NP [9] the main photoinduced effects will be due to the interaction between the electromagnetic wave and SPR excitations with additional participation of the phonon subsystem.

In the Section 2 we will give the details of AFM technique, and of tehphotoinduced treatment as well as optical birefringence detection. Section 3 will be devoted to principal results of the surface topolofy and its relation with the observed photoinduced phase changes.

2. Experimental methods

2.1. Preparation of Au NP-attached ITO

Commercially available gold colloid solutions (the diameters: 20, 30 and 40 nm) were purchased from BB International, UK. 3-aminopropyltrimethoxysilane (APTMS) was used as received from Aldrich. Indium tin oxide (ITO) coated glass substrates were the product of Geomatec Co., Ltd., Japan.

As the actual procedures to prepare AuNP-attached ITO, an ITO substrate (1.0 cm × 1.0 cm) has washed by sonicated in acetone at first, then in ethanol and in water. The ITO substrate was dried in N_2 gas, and then treated in the mixture of water, ammonium hydroxide (30%) and hydrogen peroxide (30%) (5:1:1, v/v) at 70 °C for 1.5 h. After washing with pure water and being dried in N_2 gas, the ITO was immersed in the mixture of ethanol: APTMS (100:2, v/v) overnight at 28 °C to prepare the APTMS-modified ITO. To remove residual APTMS, the APTMS-modified ITO was washed by ethanol, and finally, the APTMS-modified ITO was immersed in the colloid solution of 20 (or 40, 30) nm AuNPs for 2 h at 28 °C to prepare the AuNP-attached ITO.

2.2. AFM method

The AFM topography measurements were performed using a DIMENSION 3100 BRUCKER set working in a tapping mode. The images were then collected at ambient pressure and temperature with a commercial ARROW-NCR-20 tapping Silicon tip of apex radius less than 10 nm. These images were scanned under a digitization of 256 × 250 pixels and a scanning frequency equal to about 285 kHz. A cantilever of 42 N m^{-1} spring constant was used for that purpose.

2.3. Photoinduced treatment methods

As the photoinduced sources we have used two 10 ns lasers. The first one was Nd:YAG pulsed laser operating at wavelength 1064 nm. The second one was Er^{+3}:glass laser with fundamental laser wavelength 1540 nm. The frequency repetition of the laser beam pulsed laser was varied within the 10 ... 15 Hz. Additionally the photoinducing treatment was performed by simultaneous fundamental and doubled frequency signals. General procedure is similar to the described in the Ref. [13]. The laser power densities were varied by appropriate operating by the supply which allows perform continuous changes of the photoinducing power up to 800 MW/cm^2. Diameter of the beam was varied within the 4 ... 5 mm. Additionally the optically treated part was monitored with respect to thermo-heating using a thermocouple which was able to fix the temperature changes up to 0.1 K. The 30 mW He–Ne laser together with the lock-in optical polarimeter modulator allow to detect the changes of the birefringence at 633 nm with accuracy up to 10^{-6} [14].

The duration of the phototreatment was defined by saturation of the occurred optical phase shift. The same conditions were put for the geometry of the fundamental and doubled frequency beam. The later was achieved by BiB_3O_6 crystals cut following the phase matching conditions for the particular wavelength.

3. Results and discussion

In the Figs. 1–8 are presented surface topologies for the studied nanocomposites. The topologies are given both in the 2D as well as 3D form. For convenience of readers they are also presented in different scale. The presented results were gathered in the different parts of the surfaces in order to avoid any non-homogeneities.

For the 20 nm samples the corresponding 3D topologies are given for the 20 nm Au NP in the different scales. One can see

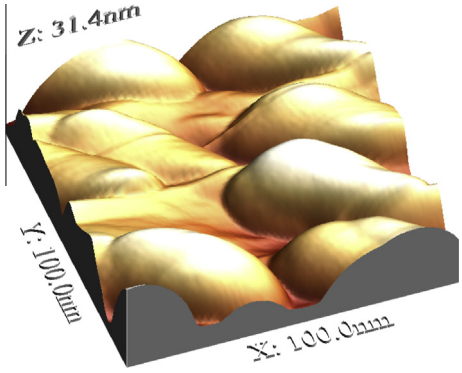

Fig. 2. AFM images of 3D topography for the 20 nm Au NP. Samples for the picture scale 100 nm × 100 nm. Measured roughness RMS: 6 nm.

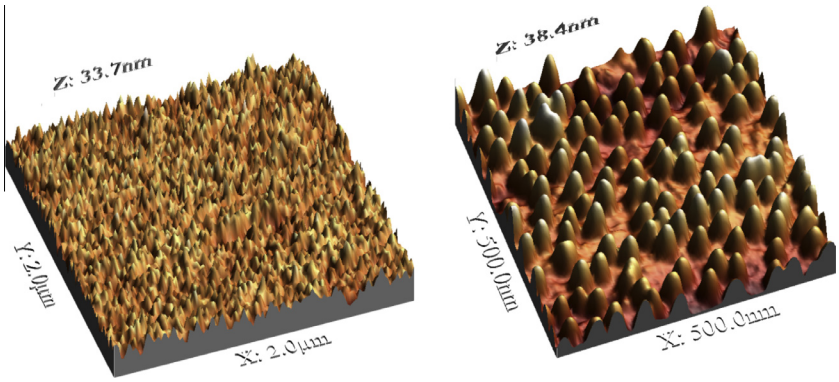

Fig. 1. AFM images of 3D topography for the 20 nm Au NP. Samples for the picture scale 2 μm × 2 μm (left) and 500 nm × 500 nm (right). Roughness parameter RMS: 4 nm (left) and 7 nm (right).

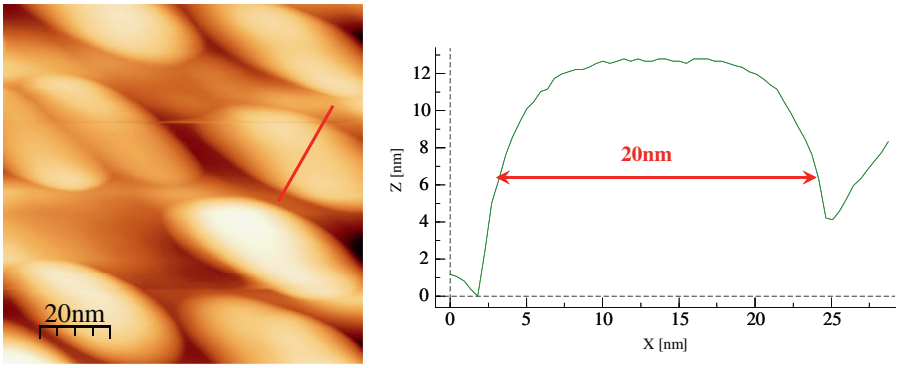

Fig. 3. Topographic AFM image as in the previous figure (left) and topography profile (right) showing the 20 nm average sizes.

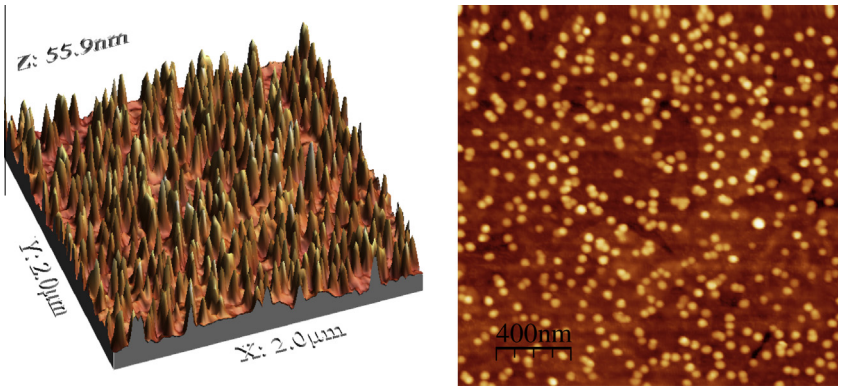

Fig. 4. Topographic AFM image as in the previous figure (left) and topography profile (right) showing the 30 nm average sizes at image sizes 2 μm × 2 μm. Roughness RMS parameter: 8.3 nm.

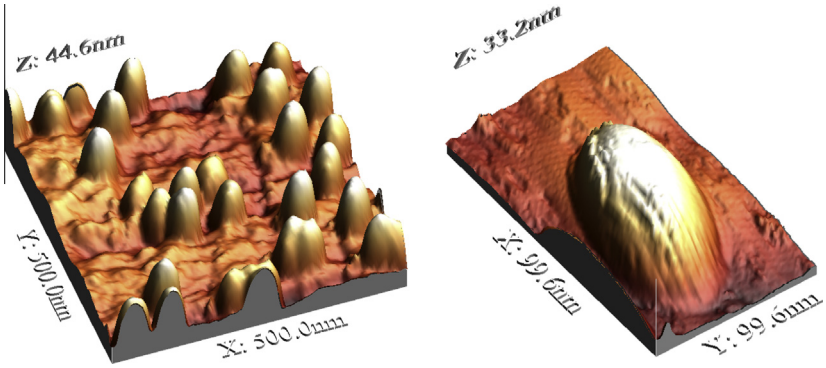

Fig. 5. 3D AFM topography of the 30 nm Au NP. For the scale 500 nm × 500 nm (left) and 100 nm × 100 nm (right) for the samples with average sizes 30 nm. The RMS roughness: 8.2 nm (left) and 7.9 nm (right).

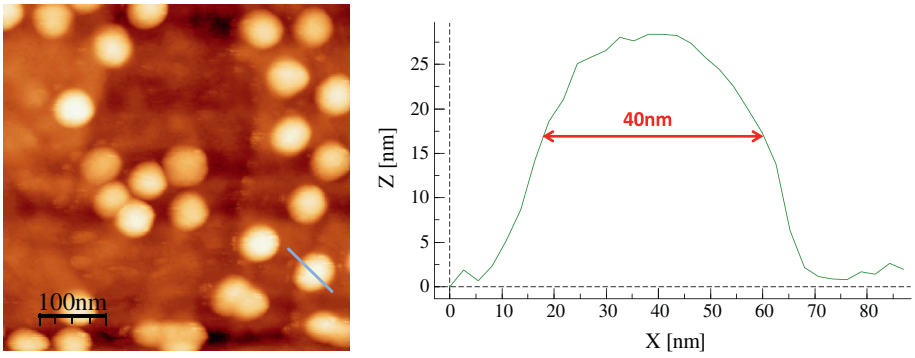

Fig. 6. 2D topographic AFM 30 nm sample (left) for image size of 500 nm and 500 nm and corresponding topographic profile (right) showing an average width of grain.

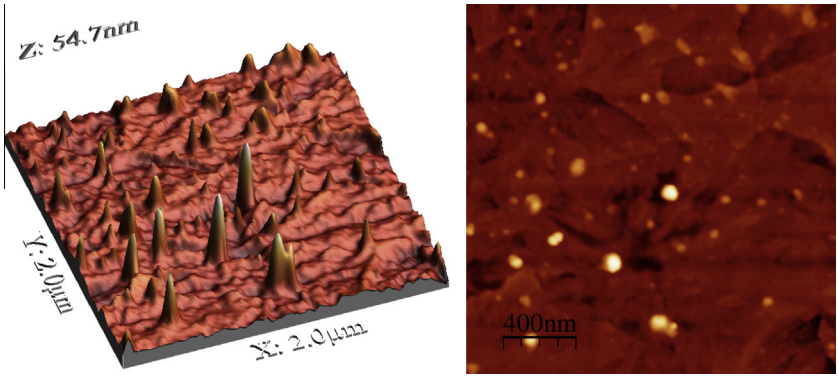

Fig. 7. 3D AFM images of 40 nm Au NP (left) and 2D image (right) for the scale 2 μm × 2 μm. Measurements roughness RMS: 3.9 nm.

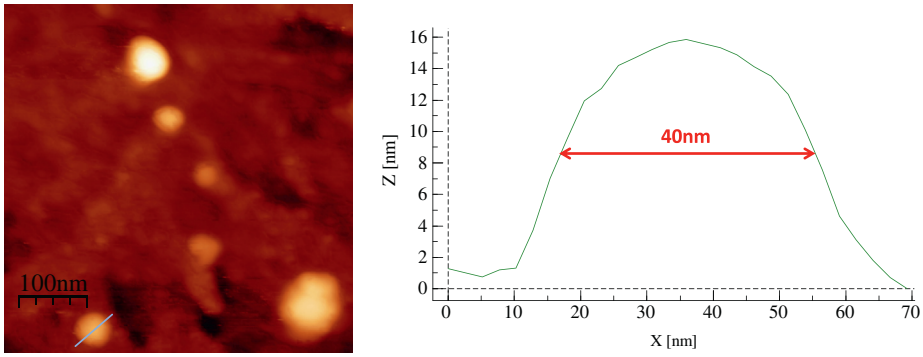

Fig. 8. AFM topography 2D image (left) and corresponding profile (right) for the 40 nm specimens for scale 500 nm × 500 nm.

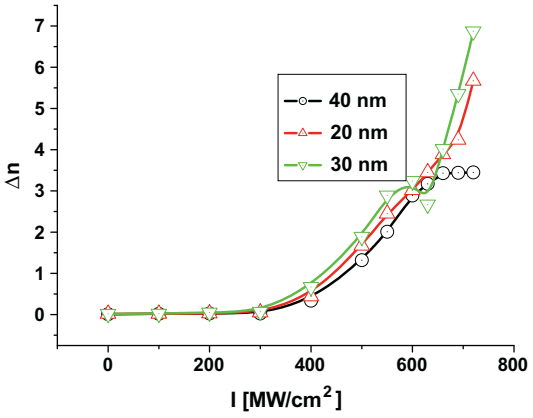

Fig. 9. Changes of the refracted index (10^{-5}) at 633 nm during the bicolor 1540 nm/770 nm Er:glass laser treatment, The results show the maximally achieved values of the photoinduced birefringence.

relatively good size mono dispersion. At the same time the inter-particle distances show any dispersion along the surface. The dispersion of the hemispherical nanograins is deviated up to 5%. Generally for these samples the aggregation is relatively low and principal role may be played by surface SPR defined by the monodispersed sizes. The inter-particle distances should not be so crucial here.

The more careful analysis of the particular hemispheres shows substantial anisotropy (see Fig. 2). This anisotropy is essential with respect to the ITO substrate. Moreover, the particular grains are not perfectly spherical, they are ellipsoidal which give additional anisotropy and there exists some degree of correlation between these grains along the surface. This factor may be crucial for the dipole–dipole and quadrupole–dipole interaction of light with the studied nanocomposites.

Following the Fig. 3 one can clearly see the sharp boarders typical for the particular grains and the profile confirms this fact. The space between the grains is clearly seen what exclude substantial role of the aggregation. The orientation of the principal axis of the ellipsoids also shows some space correlation. This one is important during the interaction of the light causing the anisotropy of the polarizability.

The situation becomes substantially different for the samples with initially incorporated 30 nm sizes. Following the Fig. 4 one can see that in this case there occurs some tendency to the aggregation. Moreover the inter-particle distances in some places are substantially different.

The more precise analysis presented in the Fig. 5 shows that they become to be like macrograins, however they may contain at least contribution of the some neighbors. The anisotropy of the ellipsoids is substantially higher. For this case there are two types of inter-grains – within the particular aggregates as well as between the different aggregates.

This is confirmed by the topo profile presented in the Fig. 6 which unambiguously shows that the grain profile is about 40 nm which is similar to the previous case, however its origin is different which clearly is shown in the Figs. 3–5.

Finally for the 40 nm samples (see Fig. 7) one can again see a good separation of the grains like for the 20 nm NP, however their sizes are substantially higher. In this case the heights of particular nanograins is relatively clear due to the slow aggregation.

The profile is the same like for the former case (see Fig. 8), however in this case there is absent any inter-particle dispersion. Because generally this grains are larger one can expect less manifestation of the interaction with the polarized light.

In the Fig. 9 is presented the dependence of the photoinduced birefringence versus the power density of the laser treatment or the case of the Er:glass laser. The effect for the Nd:YAG laser was below the noise background. One can see that for all the samples there is observed an increase of the birefringence at laser power above 350 MW/cm^2 and the angle between the beams about 28°. However for the 30 nm indicated samples the photoinduced anisotropy effect is finally the highest. It may reflect the principal role of the mentioned aggregates in the observed phenomenon. Afterwards one can see an enhancement of birefringence for the 20 nm NP where principal role may belong to the lower sizes, however due to the less polarizability these NP would be less effective. Finally as one can expect for the 40 nm the effect is less. The effect exists during the several days and decreases slowly during almost 5 days. The temperature contribution was less than 30 nm and the morphology of the surfaces was not changed after interruption of the laser treatment. So the principal role here belongs to the interaction of the bicolor polarizing light with the particular nanograins. The slow relaxation may reflect a principal role of the nanotrapping levels which trap the carriers and favoring factor here may be phonon on subsystem [15,16].

4. Conclusions

We have performed the complex studies of surface morphology and the corresponding photoinduced changes in the Au NP deposited onto the ITO substrates. We have established that maximal photoinduced effect is observed for the NP possessing the higher degree of aggregation during the treatment by 1540 nm/770 nm bicolor laser beams. for all the samples there is observed an increase of the birefringence at laser power above 350 MW/cm^2, however for the 30 nm indicated samples the photoinduced anisotropy effect is finally the highest. It may reflect the principal role of the mentioned aggregates in the observed phenomenon. Afterwards one can see an enhancement of birefringence for the 20 nm NP where principal role may belong to the lower sizes, however due to the less polarizability these NP would be less effective. Finally as one can expect for the 40 nm the effect is less. The effect exists during the several days and decreases slowly during almost 5 days.

Acknowledgements

I.V.K. and M.O. thank the Japan Society for the Promotion of Science (JSPS) for the Invitation Fellowship Program for Research in Japan (Sort Term), FY 2013.

References

[1] M. Schmid, R. Klenk, M.Ch. Lux-Steiner, M. Topic, J. Krc, Nanotechnology 22 (2011) 025204.
[2] K.R. Catchpole, A. Polman, Appl. Phys. Lett. 93 (2008) 191113.
[3] A. Centeno, J. Breeze, B. Ahmed, H. Reehal, N. Alford, Opt. Lett. 35 (2010) 76–78.
[4] T.L. Temple, H.S. Reehal, D.M. Bagnall, Sol. Energy Mater. Sol. Cells 93 (2009) 1978–1985.
[5] S. Pillai, K.R. Catchpole, T. Trupke, M.A. Green, J. Appl. Phys. 101 (2007) 093105.
[6] P. Spinelli, A. Polman, Opt. Express 20 (2012) A641–A654.
[7] I.V. Kityk, A. Umar, M. Oyama, Phys. E: Low-dimensional Syst. Nanostruct. 27 (2005) 420–426.
[8] M.K. Balakirev, V.A. Smirnov, L.I. Vostrikova, I.V. Kityk, J. Kasperczyk, W. Gruhn, J. Modern Opt. 50 (2003) 1237–1244.
[9] I.V. Kityk, J. Ebothe, I. Fuks-Janczarek, A.A. Umar, K. Kobayashi, M. Oyama, B. Sahraoui, Nanotechnology 16 (2005) 1687–1692.
[10] C.F. Bohren, D.R. Huffman, Absorption and Scattering of Light by Small Particles, Wiley-Inter-science, New York, 1983.
[11] A. Paris, A. Vaccari, A. Cala Lesina, E. Serra, L. Calliari, Plasmonics 7 (2012) 525–534.
[12] K.R. Catchpole, A. Polman, Appl. Phys. Lett. 93 (2008) 191113.
[13] M. Ghotbi, Z. Sun, A. Majchrowski, E. Michalski, I.V. Kityk, Appl. Phys. Lett. 89 (2006) 173124.
[14] G. Lemercier, C. Andraud, I.V. Kityk, J. Ebothe, B. Robertson, Chem. Phys. Lett. 400 (2004) 19–22.
[15] K. Nouneh, M. Oyama, R. Diaz, M. Abd-Lefdil, I.V. Kityk, M. Bousminta, J. Alloys Comp. 509 (2011) 2631–2638.
[16] K. Ozga, M. Oyama, M. Szota, M. Nabialek, I.V. Kityk, A. Ślęzak, A.A. Umar, K. Nouneh, J. Alloys Comp. 509 (2011) 5424–5426.